ACS APPLIED MATERIALS & INTERFACES

RESEARCH ARTICLE

www.acsami.org

Well-Defined Core−Shell Carbon Black/Polypyrrole Nanocomposites for Electrochemical Energy Storage

Chao Yang,[†] Peng Liu,*[,†] and Tingmei Wang[‡]

[†]Key Laboratory of Nonferrous Metal Chemistry and Resources Utilization of Gansu Province and State Key Laboratory of Applied Organic Chemistry, College of Chemistry and Chemical Engineering, Lanzhou University, Lanzhou 730000, China

[‡]State Key Laboratory of Solid Lubrication, Lanzhou Institute of Chemical Physics, Chinese Academy of Sciences, Lanzhou 730000, China

ABSTRACT: The well-defined core−shell carbon black/polypyrrole (CB/PPy) nanocomposites were prepared via the in situ chemical oxidative polymerization of pyrrole from the surfaces of the carbon black (CB) nanoparticles, with poly(2-hydroxy-3-(methacryloyloxy) propane-1-sulfonate) (PHMAS) as both the surfactant and the dopant. The nanocomposites exhibited the high conductivity at room temperature and the weakly temperature dependence of conductivity from 283 to 423 K. When the core−shell CB/PPy nanocomposites were used as the electrode materials for the supercapacitors, the maximum discharge capacity of 366 F/g was achieved, after being corrected for the weight percentage of the PPy phase at the current density of 5 mA/cm^2 in 1.0 M $NaNO_3$ electrolyte solution.

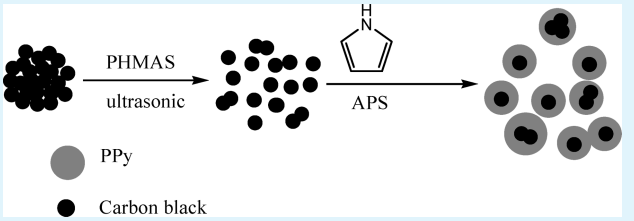

KEYWORDS: carbon black, polypyrrole, core−shell nanocomposites, electrode materials, supercapacitors

INTRODUCTION

Electrochemical capacitors (ECs), also known as supercapacitors, have attracted increasing interest as the promising energy storage devices because of their high-power energy density and longer cycle performance than the conventional dielectric capacitors.[1] The electrode is the key part of the ECs, so the electrode materials are the most important controlling factors to determine the properties of the ECs.[2] The carbon-based materials,[3] transition metal oxides,[4] and conductive polymers[5] have become the most commonly used electrode materials.

The carbon-based materials are the typical electrode materials for the electrical double layer based supercapacitors, in which energy storage is charge-separation between ions in solution and the electrified electrode/electrolyte interface, known as the electric double layer. The charge storage in such materials is limited because of the electrostatic charge storage in origin, although their cycle life is long because that their charge/discharge mechanism is governed only by the surface adsorption/desorption processes.[3]

The metal oxides and complexes have also been considered, such as RuO_2,[2] MnO_2,[6] and PbO_2.[7] However, their toxicity makes them impractical. Compared with the metal oxides, the conducting polymers have good intrinsic autoconductivity and are relatively cheap, so the preparation and fabrication costs would be more competitive. In addition, the good specific capacitance can be obtained and the existing battery-type technology may be used for the fabrication procedures. Therefore, the conducting polymers have been regarded as the promising electrode materials for supercapacitors because of their fast charge−discharge kinetics, low cost, suitable morphology, and fast doping−undoping process. With the different working principle compared with the double layer supercapacitors, the electrochemical supercapacitors exhibit a higher capacitance which produced by the rapidly doping/undoping of ions into the thin layers of the electro-active polymers. However, the conducting polymers swell and contract substantially during charge and discharge cycles. Consequently, their cycle life is poor, compared with the carbon-based supercapacitors.

There are a number of literatures on the PPy/carbon composite as the electrode materials, such as PPy/activated carbon,[8] PPy/multiwalled carbon nanotube,[9] PPy/single-walled carbon nanotube,[10] PPy/carbon foam,[11] PPy/glassy carbon,[12] PPy/carbon fiber,[13] and PPy/graphite fiber composites.[14] However, there is no report on the carbon black (CB)/conducting polymer composite electrode materials for supercapacitors by now. Being compared with other carbon materials, we select CB as the host because of its important advantages: (a) CB has the merits of the nanoscaled sizes and inexpensiveness. (b) It is an inactive inorganic host without redox characteristics, so the polymerization can be controlled easily. (c) CB and its composites have been successfully used as the conductive materials and electrode materials for supercapacitors.

In the present work, we prepared the well-defined core−shell carbon black/polypyrrole (CB/PPy) nanocomposites via the in situ chemical oxidative polymerization of pyrrole from the surfaces of the CB nanoparticles, with poly(2-hydroxy-3-(methacryloyloxy) propane-1-sulfonate) (PHMAS) as both the surfactant and the dopant. The effect of the CB feeding ratio on the electrical conductivity and temperature dependence of electrical conductivity of the composites were investigated, and the specific

Received: December 20, 2010
Accepted: February 23, 2011
Published: March 11, 2011

dx.doi.org/10.1021/am1012529 | *ACS Appl. Mater. Interfaces* 2011, 3, 1109–1114

Table 1. Surface Polymerization Conditions

samples	Py (mL)	CB (g)	CB feeding ratio (wt %)
S-1	1.0	0.0543	5
S-2	1.0	0.1147	10
S-3	1.0	0.2580	20
S-4	1.0	0.6879	40
S-5	1.0	0.9091	50
S-6	1.0	2.161	70

capacitance of the supercapacitors with the CB/PPy composites as the electrode materials was also discussed.

EXPERIMENTAL SECTION

Materials. Pyrrole monomer (Acros Organics), dehydrated with calcium hydride for 24 h, was distilled under reduced pressure before use. Ammonium peroxodisulfate (APS) (Tianjin Chemical Reagent Co., Tianjin, China) as an oxidant and sodium poly(2-hydroxy-3-(methacryloyloxy) propane-1-sulfonate) (M_n = 9590, polydispersity = 1.475, provided by the key laboratory of polymer materials of Gansu province) as the dopant and the surfactant were used as received. Sodium nitrate was purchased from Aladdin Chemical Reagent Co., Ltd. All other chemicals were analytical grade and used without further purification. The carbon black was obtained from Shanghai Fuhua Industrial Co., Ltd., China. Doubly deionized water was used throughout.

Synthesis of the PPy/CB Nanocomposites. The CB/PPy nanocomposites were prepared via the in situ surface polymerization method: A certain amount of carbon black and sodium poly(2-hydroxy-3-(methacryloyloxy) propane-1-sulfonate) (PHMAS) (5.47 g) were ultrasonically dispersed in water for 60 min to form a suspension (100 mL). In a typical procedure, pyrrole (1.0 mL) was added into the mixture under vigorous stirring at nitrogen atmosphere. Afterward, the mixture was mechanically stirred for 30 min at 0 °C. Then an aqueous solution (20 mL) containing 0.90 g of APS was added drop by drop to the above mixture to initiate the chemical oxidative polymerization. The reaction was conducted under mechanical stirring for 10 h at 0 °C. The resulting precipitates were washed with deionized water and ethanol in turn for several times. Finally, the products were dried in a vacuum at 60 °C for 24 h to obtain the desired CB/PPy nanocomposites as dark powders. The conditions of polymerization were summarized in Table 1.

Analysis and Characterizations. Raman spectra were recorded with a Fourier transform Raman (Bruker RFS 100/S) employing a 579.1 nm (Nd:YAG) laser beam. Thermogravimetric analysis (TGA) results were obtained with a TA Instrument 2050 thermogravimetric analyzer at a heating rate of 10 °C/min from 25 to 750 °C at nitrogen atmosphere.

The morphologies of the CB/PPy nanocomposites were observed using a JEM-1200 EX/S transmission electron microscope (TEM). The surface morphologies of the composites were characterized with a Philips XL-20 scanning electron microscope (SEM) (Philips Co., The Netherlands).

The surface characterization of the samples was accomplished using a PHI-5702 multifunctional X-ray photoelectron spectrometer (XPS) with pass energy of 29.35 eV and an Mg Kα line excitation source. The binding energy of C 1s (284.6 eV) was used as a reference.

The electrical conductivities of the nanocomposites were measured using SDY-4 Four-Point Probe Meter (Guangzhou Semiconductor Material Academe) at ambient temperature employing the method on a pressed pellet. The temperature dependence of conductivity was determined by WDJ-1 Temperature Change Resistance Measuring Instrument (Institute of Chemistry the Chinese Academy of Sciences) at a heating rate of 10 °C/min from 25 to 150 °C.

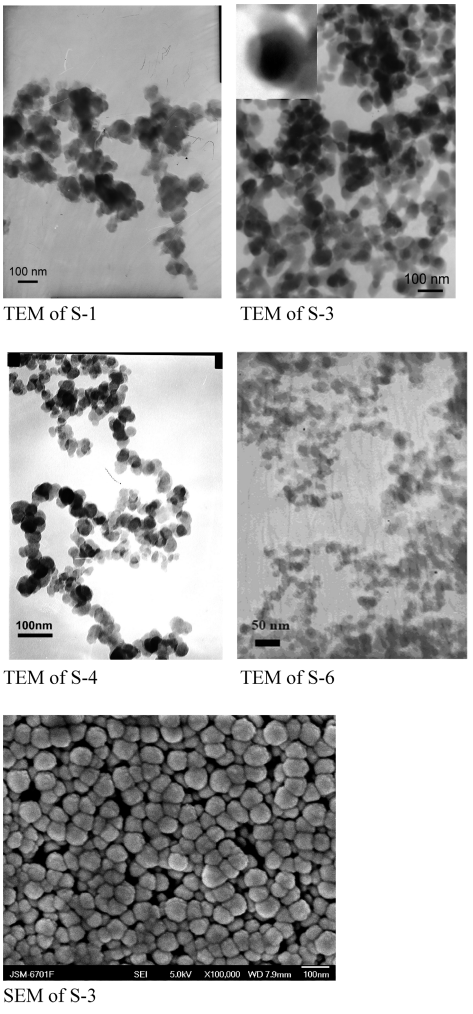

TEM of S-1 TEM of S-3

TEM of S-4 TEM of S-6

SEM of S-3

Figure 1. TEM and SEM images of the CB/PPy nanocomposites.

Electrochemical Behavior. The mixture containing 90 wt % active materials (5 mg) and 10 wt % polytetrafluoroethylene (PTFE) was well mixed in *N*,*N*-dimethylformamide (DMF) to form a slurry with proper viscosity, then the slurry was uniformly laid on a Ni foam used as a current collector (area was about 1 cm^2) and then dried at 50 °C for 24 h. The Ni foam coated with the CB/PPy nanocomposite was pressed for 1 min under 1.0 MPa. The loading mass of each sample is 5 mg. The electrolyte was 1.0 M $NaNO_3$ aqueous solution. The electrochemical behavior of the composite electrodes was evaluated by the cyclic voltammetry (CV) and the galvanostatic charge−discharge techniques. All electrochemical experiments were carried out in a three-electrode glass cell, a platinum counter electrode, and a standard calomel reference electrode (SCE). CV and galvanostatic charge−discharge tests were performed in the potential window ranged from −0.2 to 0.8 V (vs SCE) using a CHI660A electrochemical working station.

RESULTS AND DISCUSSION

Characterization of the Core−Shell CB/PPy Nanocomposites. TEM was conducted to characterize the size and shape of the presented CB/PPy nanocomposites. Figure 1 depicts the typical TEM images of the CB/PPy nanocomposites, indicating

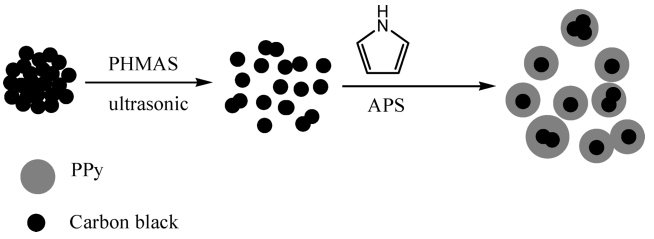

Figure 2. Schematic illustration of the synthesis process of the core−shell CB/PPy nanocomposite.

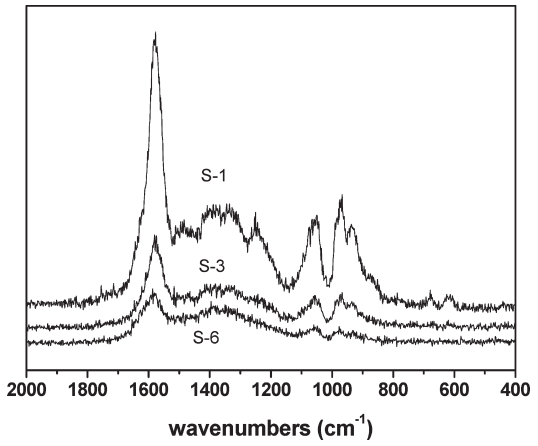

Figure 3. Raman spectra of the CB/PPy nanocomposites.

that the products are the core−shell morphology. The polypyrrole clusters and granular particles were maintained on the CB particles' surfaces even with the high feeding ratios of CB in the composites. However, the core−shell morphology could not be found for the composites with the high Py/CB feeding ratios. This is probably due to too much PPy being coated onto the CB nanoparticles and the core−shell composite nanoparticles being linked to each other with the excess polypyrrole nanoparticles.

It can be clearly observed that many PPy has located on the CB surfaces to form a shell with the diameter ranging from 30 to 100 nm. From the TEM images with higher resolutions, the core−shell structure of the nanocomposite could be observed distinctly. The SEM image illustrates that the CB/PPy nanocomposites are regular particles. The probable polymerization mechanism could be developed as in Figure 2. Because of the high adsorptive ability of the carbon black nanoparticles, the PHMAS and pyrrole had been adsorbed on the CB surfaces. Then the polymerization started after APS had been added. Thus, we can conclude that PHMAS plays the role of the dispersant as well as the dopant in the work. The particle size decreased with the increase the CB feeding ratio. It may confirm the core−shell structure of the CB/PPy nanocomposites. According to the TEM image of S-3, the composite exhibited the core−shell structure while the carbon black feeding ratio was 20%. The thin shell was barely perceptible in the TEM images with the increase the CB feeding ratio.

Figure 3 shows the Raman spectra of the CB/PPy nanocomposites in the range of 2000−400 cm^{-1}. For the CB/PPy samples, the most important absorbance peak, shown at 1600 cm^{-1}, represents the stretching mode of the C═C bonds. The double peaks at 1050 and 1080 cm^{-1} are assigned to the C−H

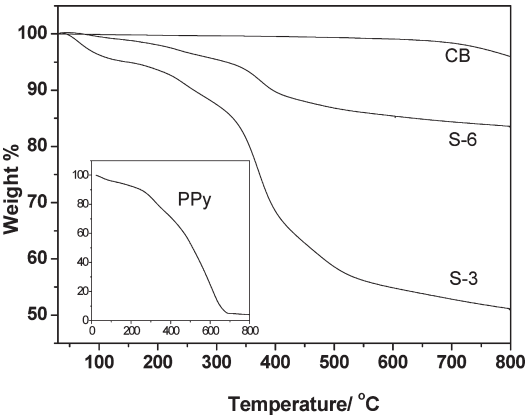

Figure 4. TGA curves of the bare CB nanoparticles, PPy, and the CB/PPy nanocomposites.

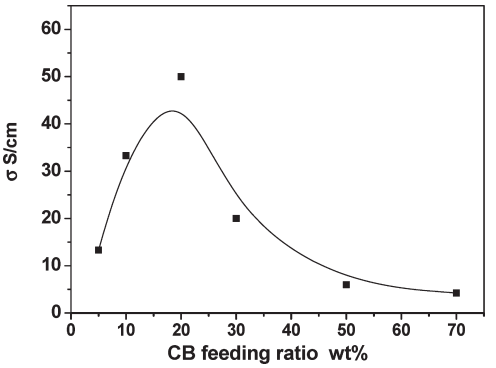

Figure 5. Conductivities of the CB/PPy nanocomposites at room temperature.

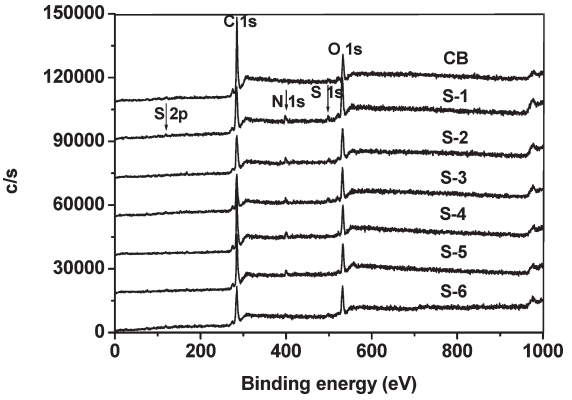

Figure 6. XPS wide scan spectra of the bare CB nanoparticles and CB/PPy nanocomposites.

in-plane deformation. The other double peaks at 1320 and 1380 cm^{-1} are attributed to the ring stretching mode of PPy.[15] Additionally, it was observed that the absorbance band intensity decreased with the increase of the CB feeding ratio.

Figure 4 illustrates the thermogravimetric analysis results of the bare CB nanoparticles, the PPy, and the core−shell CB/PPy nanocomposites. For the CB/PPy nanocomposites, a sharp loss in mass could be observed upon 300 °C and continued to 750 °C, possibly because of the large scale thermal degradation of PPy.[16]

Table 2. Surface Elemental Content from XPS Analysis

	surface element content (%)				
samples	O	C	N	S	ratio of S/N
CB	14.64	85.36	0	0	
S-1	24.90	66.14	7.04	1.93	0.274
S-2	24.25	67.21	6.95	1.59	0.229
S-3	24.30	67.86	6.51	1.33	0.204
S-4	17.44	75.14	6.11	1.31	0.214
S-5	18.60	74.54	5.63	1.23	0.218
S-6	21.92	72.58	4.30	1.20	0.279

The onset decomposition temperatures of the composites were higher than that of PPy and shifted toward the higher temperature range as the content of CB increased. This can be attributed to the retardation effect of CB as barriers for the thermal degradation of PPy.[17]

Electrical Conductivity of the Core−Shell CB/PPy Nanocomposites. The effect of the CB feeding ratio on the electrical conductivity of the CB/PPy nanocomposites is plotted in Figure 5. With the increase in CB feeding ratio, the conductivity increased first and then decreased,whereas surface elemental content ratio of S/N, obtained from the XPS analysis (Figure 6 and Table 2), decreased first and then increased, except that the surface N elemental content decreased. It indicated that the surface PPy content of the obtained core−shell CB/PPy nanocomposites decreased with the increase of the CB feeding ratio. Therefore the PPy shells changed thinner and thinner with the increase of the CB feeding ratio and the nanocomposite particles became smaller and smaller, as presented in Figure 1 (TEM images). Both the highest conductivity and the lowest doping level of PPy were achieved with 20% feeding ratio of the CB nanoparticles in S-3 sample. This is due to two main reasons: First, the compactness of the sample increased and the conducting PPy content decreased with the increase of the CB feeding ratio, which results in two contrary effects on the conductivity of the CB/PPy nanocomposite. Second, the polymeric surfactant PHMAS, which also acted as the dopant in the surface polymerization, is electrical insulative. With the higher surface elemental content ratio of S/N, more insulative PHMAS existed on the surface of the core−shell nanocomposites, so the conductivity decreased. So we can speculate that the CB nanoparticles had been encapsulated to form the core−shell structured particles, as substantiated by TEM analysis.

The temperature dependence of conductivity of the CB/PPy nanocomposites is represented in Figure 7. As the temperature increased, the conductivity increased in range of 283−423 K. The temperature dependence of conductivity clearly indicated that all the samples showed the semiconducting characteristics. However, it is worth noting that the samples with the high CB contents exhibited the weakly temperature dependence of conductivity. Figure 7 implies that the PPy contributed predominantly in the charge conduction process. The inherent disordered nature is found in the semiconducting polymers like polypyrrole. Thus the temperature dependence of conductivity σ (T) can be described by the Mott's variable range hopping (VRH) model[18]

$$\sigma(T) = \sigma_o \exp[-(T_o/T)^{\gamma}] \quad (1)$$

where σ_o is the high temperature limit of conductivity and T_o is Mott's characteristic temperature associated with the degree of

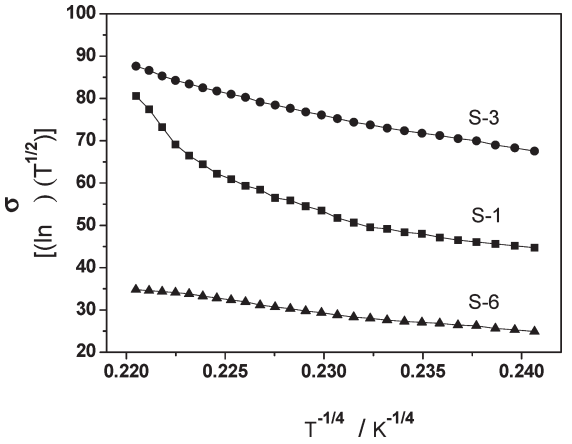

Figure 7. Temperature dependence of conductivity of the CB/PPy nanocomposites based on the VRH model.

Table 3. Weight Percentage of Polypyrrole (x %), Density of States Hopping Length R_{hop}, Activation Energy W_{hop}

sample	x (%)	R_{283K} (Å)	W_{283K} (meV)	R_{423K} (Å)	W_{423K} (meV)
S-1	95	15.5	84.2	14.1	113.9
S-3	70	4.3	23.5	3.9	31.8
S-6	30	3.7	11.4	3.3	27.5

localization of the electronic wave function. The exponent $\gamma = 1/(1 + d)$ determines the dimensionality of the conducting medium (d is defined as dimensionality). The possible values of γ are 1/4, 1/3, and 1/2 for three-, two-, or one-dimensional systems, respectively. The best fitted value of γ was obtained by the linear regression analysis. The lowest standard deviations were found for $\gamma = 1/4$ for the samples S-1, S-3, and S-6, respectively. The linear dependence of ln σ on $T^{-1/4}$, as shown in Figure 7, indicated that the three-dimensional (3D) charge transport occurred in the CB/PPy nanocomposites. However, PPy is not equipped to fine linear at ambient temperature. For the composites, as the content of PPy increased, the linearity decreased at ambient temperature. According to the VRH model, the average hopping distance R_{hop} between two sites and the activation energy W_{hop} are

$$R_{hop} = (3/8)(T_o/T)^{1/4}L \quad (2)$$

$$W_{hop} = (1/4)kT(T_o/T)^{1/4} \quad (3)$$

where L is the localization length. PPy phase and the assuming localization length of the pyrrole monomer unit is about 3 Å.[19]

At room temperature the average hopping distances for the sample S-1, S-3 and S-6, were about 15.5, 4.3, and 3.7 Å, and they reduced to about 14.1, 3.9, and 3.3 Å for the content variation of PPy. The estimated activation energies for hopping as shown in Table 3 are in the range of 113.9−11.4 meV. This implied that the decrease in the hopping distance and the increase in the hopping energy enhanced the stability of conductivity when temperature changed.

Electrochemical Studies. To further evaluate the applicability of the core−shell CB/PPy nanocomposites as the electrode materials for supercapacitors, the mass specific capacitance, the cycling performance, and the electrochemical impedance spectroscopy (EIS) of the composites have been investigated in 1.0 M

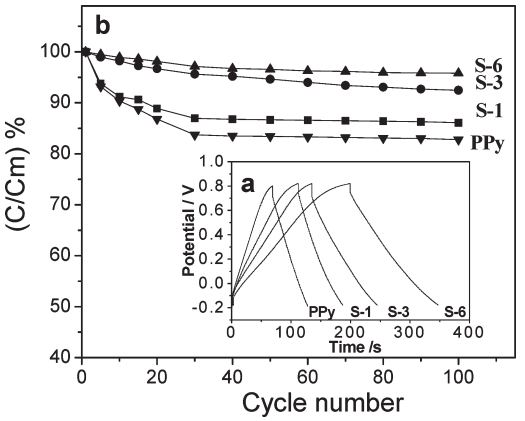

Figure 8. (a) Galvanostatic charge−discharge curves of the PPy/GNS nanocomposite electrode at a current density of 5 mA/cm^2 in 1.0 M $NaNO_3$ solution. (b) Specific capacity during galvanostatic cycles at a current density of 5 mA/cm^2 in 1.0 M $NaNO_3$ solution.

$NaNO_3$ aqueous solution. The specific capacitance (C_m) can be calculated according to eq 4

$$C_m = C/m = (I\Delta t)/(\Delta V m) \quad (4)$$

where I is the charge−discharge current, Δt is the discharge time, ΔV is the electrochemical window, and m is the mass of active material within the electrode.

The specific capacitance of the other electrode materials based on CNT/PPy or activated carbons/PPy composite was in the range of 20−500 F/g in the reported works.[10,20,21] Figure 8a shows the charge−discharge curves of PPy and the CB/PPy composite electrodes with the different CB content. The specific capacitance of PPy was 120 F/g; however, with the increase in the CB content, the specific capacitance changed from 366 F/g to 210 F/g at a current density of 5 mA/cm^2. The specific capacitance of the composite increased with the increase of the PPy loading content at the low loading densities in the curve, and reached a maximum of 366 F/g. Further increase the PPy loading content in the CB/PPy nanocomposites beyond 95 wt % resulted in a decrease. This result implies that the excess PPy did not favor the formation of the effectively dispersed PPy on the surface of the CB nanoparticles in the nanocomposites and therefore resulted in the low utilization of PPy.

The cyclic characterization was evaluated using the galvanostatic charge−discharge over 100 cycles. One can find a total loss of about 5−12% of the initial discharge capacitance was found after 40 cycles, but a fairly stable capacity was maintained thereafter, from the experimental data presented in Figure 8b. Furthermore, it indicated that CB did appear to improve the stable capacity in the view of cycle life.

To compare the power properties between the CB/PPy nanocomposites and the pure PPy, the high-rate discharge ability (A) of the electrode was also employed. The A can be obtained using eq 5[22]

$$A(\%) = C_d/C_1 \times 100\% \quad (5)$$

where C_d and C_1 are the discharge capacity of electrodes at a certain current density and 1.0 mA/cm^2, respectively. Figure 9 shows the relationship between the high-rate discharge ability and the discharge current density. It was clear from Figure 9 that the CB/PPy composite electrodes exhibited the better high-rate discharge ability, compared with the pure PPy electrode. The improved power characteristic of the composite electrodes can be deduced that the

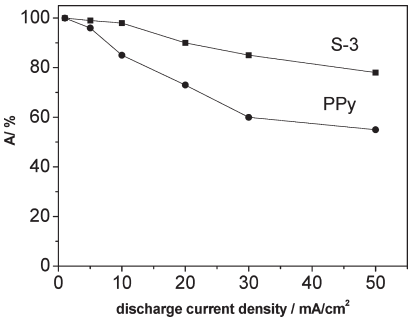

Figure 9. High-rate discharge ability for CB/PPy nanocomposite electrode and PPy.

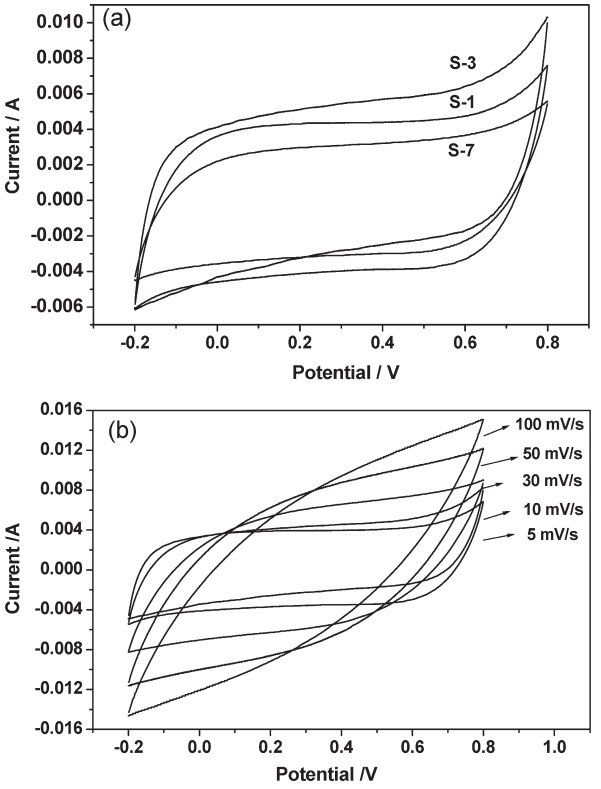

Figure 10. (a) Cyclic voltammogram curves of the CB/PPy nanocomposite electrodes at 10 mVs^{-1} in 1.0 M $NaNO_3$ solution; (b) scan rate dependence of the CB/PPy nanocomposite electrode in 1.0 M $NaNO_3$ solution.

introduction of the CB nanoparticles made the nanocomposites higher conductivity, lower charge-transfer resistance, more relative chemical durability, and therefore a better capability was obtained than the pure PPy electrode.

Figure 10a presents the cyclic voltammetry behavior of the CB/PPy composite electrodes in 1.0 M $NaNO_3$ aqueous solution. The typical rectangle-like shape of all the CV curves in Figure 10b measured at the various scan rates in 1.0 M $NaNO_3$ solution revealed the perfect electrochemical capacitive behavior of the CB/PPy nanocomposite electrodes. The curves at different scan rates show no peaks, indicating that the electrode was double-layer capacitance over the complete voltammetric cycle. However, with the scan rate increasing, the effective interaction between the ions and the electrode greatly reduced, the deviation from rectangularity of the CV became obvious.

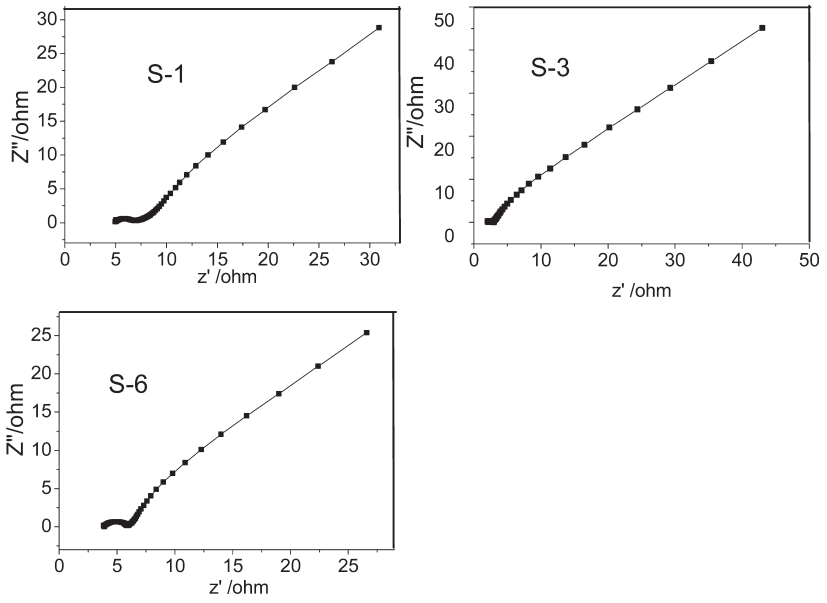

Figure 11. Impedance Nyquist plots of the CB/PPy nanocomposites.

To get more information about the ability of the CB/PPy nanocomposite electrodes in supercapacitors, EIS experiment was carried out in 1.0 M $NaNO_3$ solution at 0.4 V (vs SCE) as shown in Figure.11. There are two features for both the curves: first, in the high frequency intercept of the real axis, a solution resistance R_s can be observed. The values of the composites S-1, S-3, and S-6 were approximately 6, 3, and 8 Ω in 1.0 M $NaNO_3$ electrolyte, and this conclusion is not contrary to the previous conductivity measurements. Second, in the medium-to-low-frequency region, the unequal semicircular can be discovered from both the curves. In the low-frequency range, the impedance plots indicated a limiting diffusion process in electrolyte.[23,24]

CONCLUSIONS

In summary, we developed a novel and facile synthetic route for the preparation of the CB/PPy nanocomposites with core−shell morphology with poly(2-hydroxy-3-(methacryloyloxy) propane-1-sulfonate) as the surfactant and the dopant. The results showed that the nanocomposites exhibited the largest electrical conductivity up to 50 S/cm and the weakly temperature dependence of electrical conductivity. Furthermore, the electrochemical tests showed that the CB/PPy nanocomposites performed the typical electrochemical supercapacitive behavior and the specific capacitance of the nanocomposite electrode was approximately 366 F/g in 1.0 M $NaNO_3$ electrolyte, which allowed them to serve as ideal candidates for applications such as the antistatic coatings and electrode materials.

AUTHOR INFORMATION

Corresponding Author

*Tel.: 86-931-8912516. Fax: 86-931-8912582. E-mail: pliu@lzu.edu.cn.

ACKNOWLEDGMENT

This work was supported by the Fundamental Research Funds for the Central Universities (No. lzujbky-2011-21).

REFERENCES

(1) Conway, B. E. *Electrochemical Supercapacitors: Scientific Fundamentals and Technological Applications*; Springer-Verlag: New York, 1999.
(2) Zhang, Y.; Feng, H.; Wu, X. B.; Wang, L. Z.; Zhang, A. Q.; Xia, T. C.; Dong, H. C.; Li, X. F.; Zhang, L. S. *Int. J. Hydrogen Energy* **2009**, *34*, 4889.
(3) Frackowiak, E. *Phys. Chem. Chem. Phys.* **2007**, *9*, 1774.
(4) Hu, C. C.; Chang, K. H.; Lim, M. C.; Wu, Y. T. *Nano Lett.* **2006**, *6*, 2690–2695.
(5) Snook, G. A.; Kao, P.; Best, A. S. *J. Power Sources* **2011**, *196*, 1.
(6) Zhang, L. X.; Liu, C. S.; Zhuang, L.; Li, W. S.; Zhou, S. G.; Zhang, J. T. *Biosens. Bioelectron.* **2009**, *24*, 2825.
(7) Morris, J. M.; Jin, S.; Wang, J. Q.; Zhu, C. Z.; Urynowicz, M. A. *Electrochem. Commun.* **2007**, *9*, 1730.
(8) Muthulakshmi, B.; Kalpana, D.; Pitchumani, S. *J. Power Sources* **2006**, *158*, 1553.
(9) Jurewicz, K.; Delpeux, S.; Bertagna, V. *Chem. Phys. Lett.* **2001**, *347*, 36.
(10) An, K. H.; Jeon, K. K.; Heo, J. K. *J. Electrochem. Soc.* **2002**, *149*, 1058.
(11) Wu, Z. Q.; Zhou, X.; Yang, H. S. *J. Power Sources* **2004**, *125*, 141.
(12) Li, C. M.; Sun, C. Q.; Chen, W. *Surf. Coat. Technol.* **2005**, *198*, 474.
(13) Kim, J. H.; Lee, Y. S.; Sharma, A. K. *Electrochim. Acta* **2006**, *52*, 1727.
(14) Park, J. H.; Ko, J. M.; Park, O. O. *J. Power Sources* **2002**, *105*, 20.
(15) Liu, Y.-C.; Hwang, B.-J.; Jian, W.-J.; Sathanan, R. *Thin Solid Films* **2000**, *374*, 85.
(16) Jang, J.; Yoon, H. *Adv. Mater.* **2004**, *16*, 799.
(17) Choi, J. S.; Sung, J. H.; Choi, H. J.; Jhon, M. S. *Synth. Met.* **2005**, *153*, 129.
(18) Yoshimoto, S.; Ohashi, F; Kameyama, T. *Macromol. Rapid Commun.* **2005**, *26*, 461.
(19) Dutta, K.; De, S. K. *J. Phys. D: Appl. Phys.* **2007**, *40*, 734.
(20) Frackowiak, E.; Khomenko, V.; Jurewicz, K.; Lota, K. *J. Power Sources* **2006**, *153*, 413.
(21) Xiao, Q.; Zhou, X. *Electrochim. Acta* **2003**, *48*, 575.
(22) Wei, X.; Liu, S.; Dong, H.; Zhang, P.; Liu, Y.; Zhu, J.; Yu, G. *Electrochim. Acta* **2007**, *52*, 2423.
(23) Brousse, T.; Toupin, M.; Dugas, R.; Athouel, L.; Crosnier, O.; Belanger, D. *J. Electrochem. Soc.* **2006**, *153*, A2171.
(24) Kepas, A.; Grzeszczuk, M. *Electrochim. Acta* **2006**, *51*, 4167.